Applied Organometallic Chemistry

WILEY

Applied Organometallic Chemistry

RESEARCH ARTICLE

Diorganotin(IV) Complexes Containing Hydrazone Ligands as Prospective Bioactive Agents: Synthesis, Crystal Structure, Spectroscopic Analysis, Anticancer, and Antimicrobial Activity

Pinki Barwa[1] | Sonika Asija[1] | Yogesh Deswal[2] | Deepak Kumar[3] | Deepak Kumar Jindal[4] | Sandip Ghosh[5] | Biswarup Basu[5] | Shikha Poonia[1] | Anju Ragshaniya[1]

[1]Department of Chemistry, Guru Jambheshwar University of Science & Technology, Hisar, Haryana, India | [2]Department of Chemistry, Central University of Haryana, Mahendergarh, Haryana, India | [3]Department of Pharmaceutical Chemistry, School of Pharmaceutical Sciences, Shoolini University, Solan, India | [4]Department of Pharmaceutical Sciences, Guru Jambheshwar University of Science & Technology, Hisar, India | [5]Department of Neuroendocrinology & Experimental Hematology, Chittaranjan National Cancer Institute, Kolkata, India

Correspondence: Sonika Asija (sonika@gjust.org)

Received: 9 October 2024 | **Revised:** 22 November 2024 | **Accepted:** 16 December 2024

Funding: This work was supported by the Council of Scientific and Industrial Research, India (09/752(0120)/2021-EMR-I).

Keywords: anticancer activity | antimicrobial activity | diorganotin(IV) complexes | hydrazone ligands | single crystal XRD

ABSTRACT

The exploration of diorganotin(IV) compounds as potential inhibitors of cancer cell growth is gaining attention. Here, we have emphasized the potential of diorganotin derivatives as promising candidates for anticancer therapy. Thus, a series of Schiff base core tin(IV) complexes, including dimethyl, diethyl, dibutyl, and diphenyl derivatives, were synthesized and examined utilizing mass spectrometry, FT-IR, NMR, and single crystal XRD. The acquired spectroscopy results disclosed that hydrazone ligands connected to tin atom in a tridentate fashion *via* phenolic O, imine N, and enolic O donor atoms and formed a pentacoordinated environment, which was further validated by X-ray crystallographic diffraction study of compound **9**. Single crystal X-ray examination of compound **9** demonstrated that the Sn atom is arranged in a distorted five-coordinated square pyramidal geometry. The antimicrobial potential of all prepared compounds was examined against four bacterial and two fungal strains, and complexes **7**, **11**, and **15** having MIC values between 0.0043 and 0.0050 μmol/mL exhibit better effectiveness against *Escherichia coli* and *Candida albicans*. Further, synthesized compounds were examined for *in vitro* anticancer efficacy against MCF-7 and A549 cell lines and demonstrated substantial activity with standard Doxorubicin. Compounds **3** and **5**, being the most active, were subsequently evaluated against normal cell line HEK 293T.

1 | Introduction

Nowadays, researchers worldwide are significantly focused on the designation of antimicrobial medications due to emerging drug resistance among different microorganisms, which are responsible for many toxic illnesses and widespread epidemics in humans. Excessive consumption of antimicrobial drugs raises mortality and morbidity rates [1]. Consequently, there is a continuous demand for the development of effective microbial inhibitors.

The mortality and morbidity associated with cancer in comparison to other diseases is highly worrying. The Global Cancer Observatory (GLOBOCAN) forecasts that roughly 19.3 million new

cancer cases are predicted to be reported globally in 2020. India held the third position, following China and the United States of America. GLOBOCAN projections indicate that by 2040, the number of cancer cases in India is expected to surge to 2.08 million, marking a significant increase of 57.5% from 2020. Since the 1960s, the anticancer properties of cisplatin were discovered and the utilization of metal complexes in treating various human diseases has rapidly expanded, becoming a highly active area of research in biomedical and inorganic chemistry. Numerous platinum complexes have been synthesized, yet only a few have successfully been incorporated into chemotherapy treatments [2–4]. Platinum(II) metallocomplexes include cisplatin, nedaplatin, oxaliplatin, and carboplatin—all of which have demonstrated significant effectiveness and widespread use as anticancer drugs—because of their capacity to attach to nitrogen bases in DNA [5, 6]. Despite their great efficacy, cisplatin and its analogs suffer from significant drawbacks, including (1) limited solubility in water, (2) severe side effects linked to heavy metal poisoning, and (3) tumors developing drug tolerance. [7–9]. The latter two factors serve as the main impetus for ongoing research in the development of innovative anticancer drugs. Although platinum(II) complexes have proven to be effective in chemotherapy, because of the occurrence of severe side effects [10], resistance development, and systemic toxicity [11], researchers are looking into alternative chemotherapeutics that may have potential antitumor activity but fewer adverse effects. Initial efforts to evaluate anticancer medications based on platinum have been redirected to compounds based on nonplatinum metals [12]. Thus, to overcome the difficulties involved in employing platinum compounds as anticancer medications, a comprehensive examination of additional metals (Ti, Ge, Ga, Co, Pd, Ru, Au, and Sn) is being conducted [13, 14]. Organotin(IV) complexes have become a potent class of targeted medicines among all nonplatinum metal complexes with anticancer activity because of their lipophilicity and ability to induce apoptosis [15, 16]. These complexes have shown promise as biologically effective scaffolds and effective against malignant cell types. Currently, it is acknowledged that the harmful effects of organotin(IV) compounds operate through apoptotic mechanisms involving various pathways. These mechanisms include interacting with DNA through different binding modalities, altering Ca^{2+} homeostasis, and modulating caspase activity [17–19]. An important feature of organotin(IV) compounds is their capacity to inhibit the development of resistance in cells, potentially showing lower toxicity than cisplatin analogs [20]. Studies have shown that parameters such as the size, polarity, and number of ligands devoted to the Sn(IV) atom can significantly influence the toxicity of organotin(IV) complexes, which can vary from moderate to high. According to research findings, the number of substituents influences the sequence in which the biological efficacy of organotin compounds decreases: $> R_2Sn^{2+} > RSn^{3+}$ for R_3Sn^+ [21–24]. Careful ligand selection is a common tactic used to control the cytotoxicity of organotin(IV) compounds. These bioactive tin(IV) complexes have been created using a variety of ligands, including hydroxamic acids [25], carboxylates [26–28], cyclohexyl, and thiolate. Specifically, hydrazones, recognized for their wide biological applications such as cytotoxic [29] and antimicrobial [30] properties, when paired with Sn(IV) through the azomethine ($R_2C{=}NNR_2$) moiety, they can effectively control the proliferation of cancer cells [31, 32]. Furthermore, the selection of ligands is crucial as it influences the solubility and bioavailability of organotin(IV) complexes by transferring and leading them to the goal site.

The previously published findings regarding the biochemical and structural variety of diorganotin derivatives motivated us to develop an innovative series of diorganotin(IV) complexes. In this series, we prepared twelve new diorganotin(IV) complexes based on 2-(4-chloro-2-methylphenoxy)acetohydrazide hydrazones and extensively studied them using various spectral techniques including single crystal XRD. Additionally, the prepared compounds were investigated for *in vitro* antimicrobial and anticancer activities.

2 | Experimental

2.1 | Materials

All the chemicals, that is, 2-(4-chloro-2-methylphenoxy)acetohydrazide (98%), 5-chloro salicylaldehyde (97%), 3-ethoxy salicylaldehyde (97%), 5-bromo-3nitro salicylaldehyde (98%), and derivatives of diorganotindichloride were acquired from Sigma Aldrich. The solvents were used in their original form.

2.2 | Instrumentation

FT-IR spectra were acquired on a Perkin Elmer BX II spectrometer equipped with KBr matrix/thin sheets in 4000- to 400cm^{-1} wavenumber region. Melting points were obtained using the capillary method with GallenKamp apparatus. NMR spectra were attained on a Bruker Avance III 400-MHz spectrometer with TMS (^1H, ^{13}C) or $SnMe_4$ (^{119}Sn) as internal references, and DMSO-d_6 or $CDCl_3$ were used as solvents. TLC was applied on silica gel plates and the reaction's progress was monitored under an ultraviolet light source. On a SCIEX TripleTOF 5600+ device, mass spectra were obtained with acetonitrile serving as the solvent. An appropriate single crystal was selected and kept at 150.00(10) K during data collection. Using Olex2 [33], the structure was solved with the SHELXT [34] structure solution program using Intrinsic Phasing and refined with the SHELXL refinement package using Least Squares minimization.

2.3 | Synthesis of Hydrazone Ligands (1–3)

An equimolar methanolic solution of 2-(4-chloro-2-methylphenoxy)acetohydrazide (0.856 g, 4 mmol) was added to the methanolic solution of 5-chlorosalicylaldehyde (0.624 g, 4 mmol) for H_2L^1/3-ethoxysalicylaldehyde (0.664 g, 4 mmol) for H_2L^2 and 5-bromo-3-nitro salicylaldehyde (0.984 g, 4 mmol) for H_2L^3 and refluxed for 4–5 h with a few drops of glacial acetic acid. The white precipitates that resulted were filtered, treated with methanol, and subsequently with hexane (Scheme 1).

- H_2L^1 (**1**)

  Color: white solid; Yield: 88%; m.p.: 289°C–294°C. ^1H NMR (400 MHz, DMSO) δ: 11.62 (s, 1H, -NH), 10.35 (s, 1H, -OH), 8.49 (s, 1H, -CH=N), 8.25 (s, 1H, Ar-H), 7.72–7.64 (dd, $^3J = 4.5, 2.0$ Hz, 2H, Ar-H), 6.96–6.86 (m, 3H, Ar-H), 4.72 (s, 2H, -OCH_2), 2.21 (s, 3H, -CH_3). ^{13}C NMR (100 MHz, DMSO) δ: 162.9 (C=O), 161.5 (C-OH), 159.8 (CH=N), 149.0, 142.4, 137.1, 131.6, 129.5, 128.9, 128.2, 128.0, 112.4, 107.6, 102.5 (aromatic carbons), 69.8, 21.5 (aliphatic carbons). FT-IR

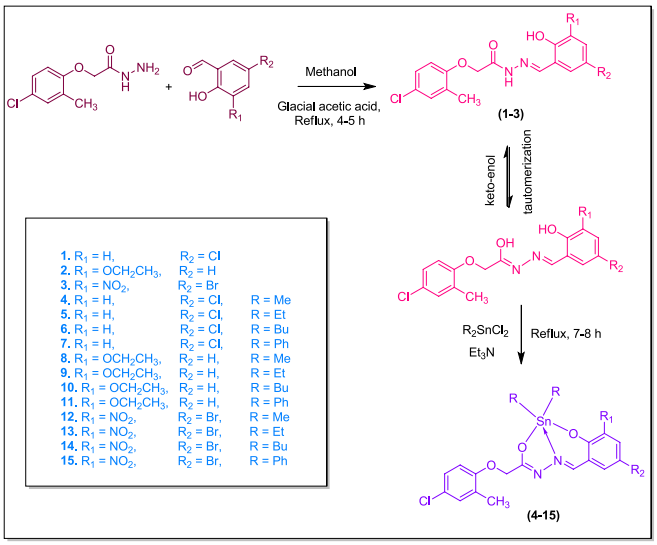

SCHEME 1 | Synthetic way of hydrazone ligands and their diorganotin(IV) complexes.

(KBr, cm^{-1}): 3433 ν(N-H), 3323 ν(O-H), 1638 ν(C=O), 1629 ν(C=N), 1076 ν(N-N). MS: calcd. 353.0455; found: 353.0410 for m/z $(M+H)^+$.

- H_2L^1 (**2**)

  Color: white solid; Yield: 85%; m.p.: 278°C–283°C. ^{1}H NMR (400 MHz, DMSO) δ: 11.56 (s, 1H, -NH), 10.64 (s, 1H, -OH), 8.52 (s, 1H, -CH=N), 8.34 (s, 1H, Ar-H), 7.30–7.12 (m, 4H, Ar-H), 7.00 (dd, ^3J = 13.1, 7.9 Hz, 1H, Ar-H), 4.72 (s, 2H, -OCH_2), 4.09–4.05 (m, 2H, OEt), 2.25 (s, 3H, -CH_3), 1.36 (d, ^3J = 5.6 Hz, 3H, OEt). ^{13}C NMR (100 MHz, DMSO) δ: 161.1 (C=O), 160.3 (C-OH), 159.7 (CH=N), 139.6, 136.6, 136.1, 130.4, 130.2, 129.1, 128.6, 126.9, 125.5, 119.4, 116.6 (aromatic carbons), 65.1, 64.3, 21.2, 15.1 (aliphatic carbons). FT-IR (KBr, cm^{-1}): 3433 ν(N-H), 3322 ν(O-H), 1640 ν(C=O), 1628 ν(C=N), 1090 ν(N-N). MS: calcd. 363.1107; found: 363.1169 for m/z $(M+H)^+$.

- H_2L^1 (**3**)

  Color: white solid; Yield: 87%; m.p.: 310°C–312°C. ^{1}H NMR (400 MHz, DMSO) δ: 12.23 (s, 1H, -NH), 11.84 (s, 1H, -OH), 8.55 (s, 1H, -CH=N), 8.30 (s, 1H, Ar-H), 8.17 (dd, ^3J = 5.1, 2.3 Hz, 2H, Ar-H), 7.26–7.19 (d, ^3J = 10.8 Hz, 2H, Ar-H), 4.77 (s, 2H, -OCH_2), 2.25 (s, 3H, -CH_3). ^{13}C NMR (100 MHz, DMSO) δ: 161.8 (C=O), 161.5 (C-OH), 159.8 (CH=N), 150.8, 149.9, 140.4, 137.1, 131.4, 128.9, 128.2, 121.9, 112.3, 107.7, 102.5 (aromatic carbons), 69.8, 21.5 (aliphatic carbons). FT-IR (KBr, cm^{-1}): 3433 ν(N-H), 3188 ν(O-H), 1641 ν(C=O), 1625 ν(C=N), 1091 ν(N-N). MS: calcd. 441.9800; found: 441.0923 for m/z $(M+H)^+$.

2.4 | Synthesis of Diorganotin(IV) Complexes (4–15)

A solution of H_2L^1 (1.059 g, 3 mmol)/H_2L^2 (1.088 g, 3 mmol)/H_2L^3 (1.327 g, 3 mmol) in tetrahydrofuran solvent was treated with triethylamine and refluxed for 30 min. After adding diphenyltindichloride (1.029 g, 3 mmol), dibutyltindichloride (0.909 g, 3 mmol), diethyltindichloride (0.741 g, 3 mmol), and dimethyltindichloride (0.657 g, 3 mmol), the reaction was refluxed for 7 to 8 h. The resulting white-colored Et_3N·HCl salt was isolated, and a rotary evaporator was employed to extract the solvent. To acquire the pure products, the resulting precipitates were recrystallized in dry hexane (Scheme 1).

- Me_2SnL^1 (**4**)

  Color: yellow solid; Yield: 86%; m.p.: 204°C–207°C. ^{1}H NMR (400 MHz, $CDCl_3$) δ: 8.55 (s, 1H, -CH=N), 7.27–7.20 (m, 1H, Ar-H), 7.19–7.05 (m, 3H, Ar-H), 6.79 (t, ^3J = 8.5 Hz, 1H, Ar-H), 6.70 (d, ^3J = 9.0 Hz, 1H, Ar-H), 4.65 (s, 2H, -OCH_2), 2.28 (s, 3H, -CH_3), 0.80 (s, 6H, Me). ^{13}C NMR (100 MHz, $CDCl_3$) δ: 167.6 (C=O), 165.6 (C-OH), 163.0 (CH=N), 139.4, 138.5, 136.5, 133.3, 130.4, 128.7, 124.3, 121.6, 118.5, 118.5, 111.8 (aromatic carbons), 65.4, 21.8 (aliphatic carbons), 1.7 (Sn-Me). ^{119}Sn NMR (400 MHz, $CDCl_3$) δ: −128. FT-IR (KBr, cm^{-1}): 1614 ν(C=N), 1036 ν(N-N), 577 ν(Sn-O), 474 ν(Sn-N). MS: calcd. 500.9790; found: 500.9795 for m/z $(M+H)^+$.

- Et_2SnL^1 (**5**)

  Color: pale yellow solid; Yield: 82%; m.p.: 240°C–244°C. ^{1}H NMR (400 MHz, $CDCl_3$) δ: 8.58 (s, 1H, -CH=N), 7.12 (d, ^3J = 13.2 Hz, 4H), 6.83–6.74 (dd, ^3J = 35.9, 7.6 Hz, 2H), 4.68 (s, 2H, -OCH_2), 2.29 (s, 3H, -CH_3), 1.49–1.39 (m, 4H, Et), 1.25 (d, ^3J = 7.2 Hz, 6H, Et). ^{13}C NMR (100 MHz, $CDCl_3$) δ: 168.3 (C=O), 166.5 (C-OH), 164.8 (CH=N), 159.6, 157.4, 141.8, 138.8, 137.9, 136.3, 130.3, 128.7, 124.3, 119.3, 118.0, 111.8, 107.6 (aromatic carbons), 65.7, 22.6 (aliphatic carbons), 14.2, 9.5 (Sn-Et). ^{119}Sn NMR (400 MHz, $CDCl_3$) δ: −166. FT-IR (KBr, cm^{-1}): 1616 ν(C=N), 1030 ν(N-N), 555 ν(Sn-O), 462 ν(Sn-N). MS: calcd. 529.0103; found: 529.0111 for m/z $(M+H)^+$.

- Bu_2SnL^1 (**6**)

  Color: light yellow solid; Yield: 77%; m.p.: 257°C–263°C. ^{1}H NMR (400 MHz, $CDCl_3$) δ: 8.63 (s, 1H, -CH=N), 7.13–7.06 (m, 2H, Ar-H), 6.96 (d, ^3J = 6.6 Hz, 1H, Ar-H), 6.82 (dd, ^3J = 18.2, 7.9 Hz, 2H, Ar-H), 6.64 (t, ^3J = 7.3 Hz, 1H, Ar-H), 4.67 (s, 2H, -OCH_2), 2.29 (s, 3H, -CH_3), 1.53–1.32 (ddd,

^3J = 45.0, 31.8, 10.8 Hz, 12H, Bu), 0.88–0.84 (t, ^3J = 6.5 Hz, 6H, Bu). ^{13}C NMR (100 MHz, $CDCl_3$) δ: 169.2 (C=O), 168.7 (C-OH), 165.0 (CH=N), 141.0, 136.3, 135.6, 130.7, 128.9, 128.6, 128.1, 127.6, 127.4, 111.0, 107.3 (aromatic carbons), 66.0, 22.1 (aliphatic carbons), 26.8, 26.3, 13.6, 8.6 (Sn-Bu). ^{119}Sn NMR (400 MHz, $CDCl_3$) δ: −166. FT-IR (KBr, cm^{-1}): 1604 ν(C=N), 1024 ν(N-N), 571 ν(Sn-O), 466 ν(Sn-N). MS: calcd. 585.0729; found: 585.0720 for *m/z* $(M+H)^+$.

- Ph_2SnL^1 (**7**)

  Color: dusky yellow solid; Yield: 80%; m.p.: 383°C–387°C. ^{1}H NMR (400 MHz, $CDCl_3$) δ: 8.55 (s, 1H, -CH=N), 7.82–7.60 (m, 4H, Ar-H), 7.47–7.35 (m, 7H, Ar-H), 7.22–7.13 (m, 2H, Ar-H), 7.06 (d, ^3J = 8.9 Hz, 2H, Ar-H), 6.84 (d, ^3J = 8.7 Hz, 1H, Ar-H), 4.84 (s, 2H, -OCH_2), 2.36 (s, 3H, -CH_3). ^{13}C NMR (100 MHz, $CDCl_3$) δ: 169.1 (C=O), 168.3 (C-OH), 165.2 (CH=N), 141.4, 139.3, 136.2, 135.8, 130.5, 130.4, 129.0, 128.8, 128.7, 128.6, 128.2, 127.7, 127.6, 111.1, 107.8, 105.2, 103.8 (aromatic carbons), 66.0, 21.6 (aliphatic carbons). ^{119}Sn NMR (400 MHz, $CDCl_3$) δ: −309. FT-IR (KBr, cm^{-1}): 1615 ν(C=N), 1030 ν(N-N), 571 ν(Sn-O), 470 ν(Sn-N). MS: calcd. 625.0103; found: 625.0115 for *m/z* $(M+H)^+$.

- Me_2SnL^2 (**8**)

  Color: light yellow solid; Yield: 82%; m.p.: 242°C–247°C. ^{1}H NMR (400 MHz, $CDCl_3$) δ: 8.61 (s, 1H, -CH=N), 8.00 (d, ^3J = 2.2 Hz, 1H, Ar-H), 7.48 (d, ^3J = 2.1 Hz, 1H, Ar-H), 7.14–6.99 (dd, ^3J = 33.3, 24.6 Hz, 3H, Ar-H), 6.78 (d, ^3J = 8.7 Hz, 1H, Ar-H), 4.69 (s, 2H, -OCH_2), 4.14–4.09 (dd, ^3J = 13.5, 6.7 Hz, 2H, OEt), 2.28 (s, 3H, -CH_3), 1.44–1.39 (m, 2H, OEt), 0.89 (s, 6H, -CH_3). ^{13}C NMR (100 MHz, $CDCl_3$) δ: 168.7 (C=O), 165.0 (C-OH), 160.5 (CH=N), 141.1, 136.2, 135.6, 128.9, 128.6, 128.2, 127.6, 127.4, 110.9, 107.6, 104.7 (aromatic carbons), 65.1, 63.5, 21.5, 14.1 (aliphatic carbons), 1.4 (Sn-Me). ^{119}Sn NMR (400 MHz, $CDCl_3$) δ: −130.88. FT-IR (KBr, cm^{-1}): 1596 ν(C=N), 1042 ν(N-N), 586 ν(Sn-O), 474 ν(Sn-N). MS: calcd. 511.0442; found: 511.0333 for *m/z* $(M+H)^+$.

- Et_2SnL^2 (**9**)

  Color: yellow solid; Yield: 78%; m.p.: 262°C–267°C. ^{1}H NMR (400 MHz, $CDCl_3$) δ: 8.66 (s, 1H, -CH=N), 7.13–7.08 (dd, ^3J = 15.3, 6.6 Hz, 2H), 6.96 (d, ^3J = 7.4 Hz, 1H), 6.85–6.80 (dd, ^3J = 18.8, 8.2 Hz, 2H), 6.65 (t, ^3J = 7.8 Hz, 1H), 4.67 (s, 2H, -OCH_2), 4.14–4.09 (q, ^3J = 7.0 Hz, 2H, OEt), 2.29 (s, 3H, -CH_3), 1.50 (dd, ^3J = 13.7, 7.3 Hz, 4H, Et), 1.41 (s, 3H, OEt), 1.25 (t, ^3J = 8.0 Hz, 6H, Et). ^{13}C NMR (100 MHz, $CDCl_3$) δ: 169.4 (C=O), 165.0 (C-OH), 160.5 (CH=N), 141.0, 136.3, 135.6, 128.9, 128.6, 128.1, 127.6, 127.4, 111.0, 107.3, 104.5 (aromatic carbons), 66.9, 65.9, 21.5, 15.5 (aliphatic carbons), 14.2, 9.3 (Sn-Et). ^{119}Sn NMR (400 MHz, $CDCl_3$) δ: −168. FT-IR (KBr, cm^{-1}): 1598 ν(C=N), 1032 ν(N-N), 545 ν(Sn-O), 467 ν(Sn-N). MS: calcd. 539.0755; found: 539.0996 for *m/z* $(M+H)^+$.

- Bu_2SnL^2 (**10**)

  Color: light yellow solid; Yield: 78%; m.p.: 274°C–278°C. ^{1}H NMR (400 MHz, $CDCl_3$) δ: 8.63 (s, 1H, -CH=N), 7.13–7.05 (m, 2H, Ar-H), 6.96 (d, ^3J = 7.1 Hz, 1H, Ar-H), 6.85–6.80 (dd, ^3J = 18.0, 8.1 Hz, 2H, Ar-H), 6.65 (t, ^3J = 7.7 Hz, 1H, Ar-H), 4.67 (s, 2H, -OCH_2), 4.09 (dd, ^3J = 13.5, 6.7 Hz, 2H, OEt), 2.29 (s, 3H, -CH_3), 1.53–1.51 (dd, ^3J = 26.8, 6.9 Hz, 8H, Bu), 1.41 (t, ^3J = 6.8 Hz, 3H, OEt), 1.31 (dd, ^3J = 14.8, 7.6 Hz, 4H, Bu), 0.86 (t, ^3J = 7.1 Hz, 6H, Bu). ^{13}C NMR (100 MHz, $CDCl_3$) δ: 169.7 (C=O), 166.6 (C-OH), 165.4 (CH=N), 150.7, 148.7, 136.1, 135.8, 135.2, 128.6, 128.2, 127.6, 107.7, 104.5, 103.8 (aromatic carbons), 66.9, 66.0, 22.7, 14.5 (aliphatic carbons), 29.7, 25.0, 14.1, 9.2 (Sn-Bu). ^{119}Sn NMR (400 MHz, $CDCl_3$) δ: −170. FT-IR (KBr, cm^{-1}): 1605 ν(C=N), 1030 ν(N-N), 590 ν(Sn-O), 443 ν(Sn-N). MS: calcd. 595.1381; found: 595.0816 for *m/z* $(M+H)^+$.

- Ph_2SnL^2 (**11**)

  Color: dark yellow solid; Yield: 80%; m.p.: 363°C–367°C. ^{1}H NMR (400 MHz, $CDCl_3$) δ: 8.65 (s, 1H, -CH=N), 7.80–7.67 (m, 4H, Ar-H), 7.50–7.43 (m, 7H, Ar-H), 7.33–7.21 (m, 2H, Ar-H), 7.08 (m, 2H, Ar-H), 6.95 (d, ^3J = 8.6 Hz, 1H, Ar-H), 4.89 (s, 2H, -OCH_2), 4.06 (dd, ^3J = 12.5, 5.7 Hz, 2H, OEt), 2.42 (s, 3H, -CH_3), 1.46 (t, ^3J = 8.8 Hz, 3H, OEt). ^{13}C NMR (100 MHz, $CDCl_3$) δ: 169.6 (C=O), 168.1 (C-OH), 165.3 (CH=N), 139.2, 136.5, 136.2, 135.9, 133.3, 131.0, 130.4, 128.8, 128.7, 128.3, 128.2, 127.7, 127.6, 111.1, 107.9, 105.2, 103.8 (aromatic carbons), 66.9, 65.9, 21.3, 15.3 (aliphatic carbons). ^{119}Sn NMR (400 MHz, $CDCl_3$) δ: −303. FT-IR (KBr, cm^{-1}): 1610 ν(C=N), 1046 ν(N-N), 566 ν(Sn-O), 452 ν(Sn-N). MS: calcd. 635.0755; found: 609.1315 for *m/z* $(M+H)^+$.

- Me_2SnL^3 (**12**)

  Color: bright yellow solid; Yield: 86%; m.p.: 249°C–252°C. ^{1}H NMR (400 MHz, $CDCl_3$) δ: 8.62 (s, 1H, -CH=N), 8.02 (d, ^3J = 1.9 Hz, 1H, Ar-H), 7.48 (d, ^3J = 1.1 Hz, 1H, Ar-H), 7.28–7.06 (m, 2H, Ar-H), 6.79 (d, ^3J = 8.6 Hz, 1H, Ar-H), 4.70 (s, 2H, -OCH_2), 2.29 (s, 3H, -CH_3), 0.90 (s, 6H, Me). ^{13}C NMR (100 MHz, $CDCl_3$) δ: 168.7 (C=O), 165.0 (C-OH), 160.5 (CH=N), 141.1, 136.2, 135.6, 130.5, 128.9, 128.6, 127.6, 127.4, 110.9, 107.6, 104.7 (aromatic carbons), 66.8, 22.7 (aliphatic carbons), 2.3 (Sn-Me). ^{119}Sn NMR (400 MHz, $CDCl_3$) δ: −132. FT-IR (KBr, cm^{-1}): 1599 ν(C=N), 1029 ν(N-N), 576 ν(Sn-O), 456 ν(Sn-N). MS: calcd. 589.9135; found: 590.0003 for *m/z* $(M+H)^+$.

- Et_2SnL^3 (**13**)

  Color: pale yellow solid; Yield: 78%; m.p.: 284°C–289°C. ^{1}H NMR (400 MHz, $CDCl_3$) δ: 8.64 (s, 1H, -CH=N), 8.02 (d, ^3J = 28.9 Hz, 1H, Ar-H), 7.47 (s, 1H, Ar-H), 7.14–7.08 (m, 2H, Ar-H), 6.79 (d, ^3J = 8.7 Hz, 1H, Ar-H), 4.70 (s, 2H, -OCH_2), 2.28 (s, 3H, -CH_3), 1.60–1.54 (dd, ^3J = 15.4, 7.6 Hz, 4H, Bu), 1.29–1.24 (m, 6H, Bu). ^{13}C NMR (100 MHz, $CDCl_3$) δ: 169.9 (C=O), 165.7 (C-OH), 162.3 (CH=N), 149.2, 136.1, 136.0, 128.6, 128.2, 127.6, 110.7, 107.9, 104.5, 103.8, 103.7 (aromatic carbons), 66.8, 22.1 (aliphatic carbons), 14.6, 9.2 (Sn-Et). ^{119}Sn NMR (400 MHz, $CDCl_3$) δ: −170. FT-IR (KBr, cm^{-1}): 1609 ν(C=N), 1036 ν(N-N), 581 ν(Sn-O), 442 ν(Sn-N). MS: calcd. 617.9448; found: 617.9918 for *m/z* $(M+H)^+$.

- Bu_2SnL^3 (**14**)

  Color: yellow solid; Yield: 73%; m.p.: 245°C–247°C. ^{1}H NMR (400 MHz, $CDCl_3$) δ: 8.60 (s, 1H, -CH=N), 8.36–8.27 (d, ^3J = 35.5 Hz, 1H, Ar-H,), 8.02 (d, ^3J = 1.6 Hz, 1H, Ar-H), 7.47 (d, ^3J = 1.5 Hz, 1H, Ar-H), 7.14 (s, 1H, Ar-H), 6.79 (d, ^3J = 8.6 Hz, 1H, Ar-H), 4.70 (s, 2H, -OCH_2), 2.29 (d, ^3J = 10.2 Hz, 3H, -CH_3), 1.58–1.28 (m, 12H, Bu), 0.88 (t, ^3J = 7.3 Hz, 6H, Bu). ^{13}C NMR (100 MHz, $CDCl_3$) δ: 169.9

(C=O), 165.7 (C-OH), 162.3 (CH=N), 149.2, 136.1, 136.0, 128.6, 128.2, 127.6, 110.7, 107.9, 104.5, 103.8, 103.7 (aromatic carbons), 66.8, 22.1 (aliphatic carbons), 27.7, 25.2, 14.6, 9.2 (Sn-Bu). ^{119}Sn NMR (400 MHz, $CDCl_3$) δ: −167. FT-IR (KBr, cm^{-1}): 1610 ν(C=N), 1045 ν(N-N), 572 ν(Sn-O), 467 ν(Sn-N). MS: calcd. 674.0074; found: 602.0789 for *m/z* $(M+H)^+$.

- Ph_2SnL^3 (**15**)

  Color: yellow solid; Yield: 84%; m.p.: 390°C–393°C. ^{1}H NMR (400 MHz, $CDCl_3$) δ: 8.60 (s, 1H, -CH=N), 8.16 (d, ^3J = 2.0 Hz, 1H, Ar-H), 8.01–8.00 (m, 1H, Ar-H), 7.73 (d, ^3J = 6.8 Hz, 3H, Ar-H), 7.51–7.39 (m, 6H, Ar-H), 7.22–7.12 (s, 1H, Ar-H), 7.08 (d, ^3J = 6.6 Hz, 1H, Ar-H), 7.03–6.94 (m, 1H, Ar-H), 6.85 (d, ^3J = 8.7 Hz, 1H, Ar-H), 4.91 (s, 2H, -OCH_2), 2.37 (s, 3H, -CH_3). ^{13}C NMR (100 MHz, $CDCl_3$) δ: 169.8 (C=O), 165.7 (C-OH), 161.6 (CH=N), 151.2, 149.0, 138.9, 136.4, 136.1, 136.1, 135.8, 135.1, 130.6, 128.9, 128.7, 128.3, 127.7, 110.9, 108.2, 105.2, 103.8 (aromatic carbons), 66.9, 22.2 (aliphatic carbons). ^{119}Sn NMR (400 MHz, $CDCl_3$) δ: −307. FT-IR (KBr, cm^{-1}): 1614 ν(C=N), 1035 ν(N-N), 565 ν(Sn-O), 467 ν(Sn-N). MS: calcd. 713.9448; found: 713.9532 for *m/z* $(M+H)^+$.

2.5 | Antimicrobial Potency

Synthesized compounds were evaluated using a previously published procedure to study their antimicrobial activity [35–37].

2.6 | Anticancer Activity

2.6.1 | Cell Culture

To examine the cytotoxic potential of the substances, three cell types were selected: A549, which originated from human alveolar adenocarcinoma epithelial cells (ATCC No. CCL-185); MCF7, which originated from human breast cancer cells (ATCC No. HTB-22); and HEK 293T, which originated from normal human embryonic kidney cells (ATCC No. CRL-3216). The cells were sustained at 37°C with 5% CO_2 in a moistened incubator in Dulbecco's modified Eagle medium (DMEM) supplemented using 10% fetal bovine serum (FBS) and 1% penicillin–streptomycin.

2.6.2 | Cytotoxicity Assay

A549, MCF7, and HEK 293T cells were grown in DMEM culture media enriched with 10% FBS and 1% penicillin–streptomycin. A humidified incubator was used to maintain the cells at 37°C and 5% CO_2. For the experiment, approximately 1000 cells per well were sown in a 96-well tissue culture plate with growth phase cells. To create a high-concentration stock solution, test compounds were dissolved in DMSO, and repeated dilutions were performed to produce varied concentrations adequate for the assay. The cells were seeded for 24 h, and then they were treated for 48 h with various compounds at varying doses. The hydrazone ligands (**1–3**) and their organotin(IV) derivatives (**4–15**) were applied in μM concentrations. All test compounds were applied in four different concentrations of 5, 10, 25, and 50 μM with corresponding untreated group. Following a 48-h treatment period, add 10 μL/well of MTT reagent at a final concentration of 5 mg/mL, and then incubate the plate to produce formazan crystals. DMSO was employed for the dissolution of formazan crystals. A microplate reader was employed to determine the absorbance at 570 nm with a standard wavelength of 650 nm. Cell viability percentages were computed by comparing absorbance readings of treated wells with controls, and a dose–response curve was used to plot the IC_{50} value, which indicates the quantity of chemicals that cause a 50% reduction in cell viability [38–41].

3 | Outcomes and Discussion

3.1 | Synthetic Procedures

Hydrazone ligands, $H_2L^{1–3}$ (**1–3**), were synthesized *via* refluxing a methanolic solution of 2-(4-chloro-2-methylphenoxy)acetohydrazide with salicylaldehyde derivatives. Moreover, the obtained ligands were reacted with R_2SnCl_2 in an equimolar ratio to synthesize 12 diorganotin(IV) complexes, $R_2SnL^{1–3}$ (**4–15**). Several spectroscopic approaches demonstrate the tin metal atom to be pentacoordinated, suggesting that hydrazone ligands coordinate to it through ONO donor atoms. Furthermore, they exhibited solubility in DMF, THF, and DMSO solvents.

3.2 | ^{1}H NMR

Analysis of ^{1}H NMR spectra can be used to effectively monitor the synthesis of hydrazone ligands and their diorganotin(IV) complexes. In hydrazone ligands, the signal for azomethine protons at δ 8.55–8.49 ppm along with the occurrence of signal for -NH and-OH groups at δ 12.23–11.56 ppm and δ 11.84–10.35 ppm indicated the establishment of hydrazone ligand. The lack of signals in the diorganotin(IV) complex's spectra corresponding to the -OH and -NH groups designates that the ligands have been deprotonated and enolized, which specifies their coordination to the diorganotin(IV) centers. In the spectra of diorganotin(IV) complexes, azomethine protons experience a downfield shift because of the deshielding effect instigated by the attachment of the nitrogen atom with the tin(IV) metal center [42]. The signals due to ethoxy protons in ligand **2** were observed at δ 4.09–4.05 ppm and δ 1.36 ppm and exhibited negligible shift on complexation as compared with the ligands, demonstrating that ethoxy protons are not engaged in coordination. A coordination link between the nitrogen of the azomethine and the Sn(IV) center was demonstrated by the discrete tin satellite peaks that arise from the interaction of the azomethine proton and the Sn(IV) center with a $^3J(^{119}Sn\text{-}^1H)$ value of 60–66 Hz [43]. In complexes **4**, **8**, and **12**, the spectra show resonance signals with tin satellite peaks around δ 0.90–0.80 ppm, which support the coordination of the dimethytin(IV) moiety. Complexes **5**, **9**, and **13** exhibit a resonance signal in the region of δ 1.57–1.39 and δ 1.29–1.24 ppm, confirming the coordination of the diethyl(IV) moiety. Complexes **6**, **10**, and **14** include the dibutyl moiety, as evidenced by additional signals at δ 1.60–1.28 and δ 0.88–0.86 ppm along with distinctive multiplicity. Likewise, the resonance signals that appear in the δ 8.05- to 6.84-ppm region of the spectra of complexes **7**, **11**, and **15** validate the binding of the diphenyltin(IV) moiety [44, 45]. Figures S1–S14 provide the obtained

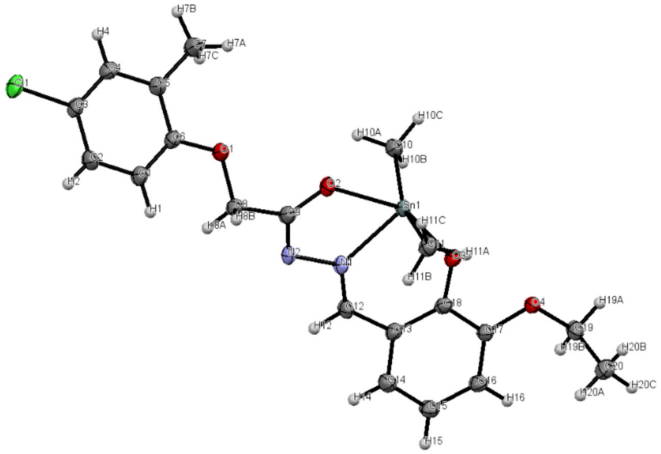

FIGURE 1 | A 50% probability level ORTEP graphic of compound **9**.

results. Furthermore, Lockhart's equation [46] was used to calculate the value of θ, which yields a value of 122.65°–134.48° and confirms penta coordination. The outcomes are consistent with the previously reported diorganotin(IV) complexes.

3.3 | ^{13}C NMR

^{13}C NMR spectroscopy provides additional evidence to support the ^{1}H NMR results. A strong indication of Schiff base formation was the presence of the signal attributed to -C=O, C-OH, and -CH=N groups in the regions of δ 162.9–161.1, δ 161.5–160.3, and δ 159.8–159.7 ppm, respectively, in the spectra of ligands. These groups exhibit a notable downfield shift in their diorganotin(IV) complexes because of their binding with tin metal core [47]. The carbon atoms of the diphenyl, dibutyl, diethyl, and dimethyl moieties were discernible in the appropriate regions in the spectra of complexes. The existence of a resonance signal in the spectra of dimethyl complexes at δ 2.3–1.4 ppm indicates the coordination of methyl groups. The presence of a signal at δ 14.6–9.2 ppm signifies the coordination of ethyl groups in diethyl complexes. The coordination of the dibutyl moiety is indicated by the presence of four extra resonance signals at δ 27.7–8.6 ppm. In the distinctive aromatic region, six more resonance signals show that the diphenyl moiety is coordinated. Figures S15–S29 summarizes the observed data. A five-coordinated geometry is evident from the measured values of ^{1}J[^{119}Sn-^{13}C] for complexes, which were found in the 602 to 650 Hz range [48]. Additionally, the values of θ, i.e. C-Sn-C = 130.5° and 134.0°, determined for complexes using J. HoleNcek's derivation also enable five coordination [49].

3.4 | ^{119}Sn NMR

To obtain further confirmation regarding the coordination geometry of diorganotin(IV) complexes, ^{119}Sn NMR spectroscopy was used. There is a clear correlation between the number of coordinating molecules surrounding the Sn(IV) core and the chemical shift values of ^{119}Sn NMR. The presence of electron-releasing alkyl groups induce steric crowding around the tin center, leading to shielding effects and resulting in an upfield shift. For diorganotin(IV) complexes, the chemical shift values were found in the range from δ −128 to −309 ppm [50, 51]. The acquired data are condensed in Figures S30–S33. The chemical shift values of ^{119}Sn NMR for the complexes lie within the range that suggests five-coordinate geometry.

3.5 | FT-IR Spectroscopy

FT-IR spectra of synthesized ligands and diorganotin(IV) complexes were obtained in the 4000–400 cm^{-1} wavenumber range. The lack of distinct bands at 3433 cm^{-1} for ν(OH) and 3323–3188 cm^{-1} for ν(NH) in the spectra of all prepared complexes proposes the formation of diorganotin(IV) complexes. The hydrazones displayed characteristic stretching bands between 1669 and 1664 cm^{-1} for ν(C=O), which also shifted as complex formed. These observations indicated that the ligands were tautomerized to enol form during the complexation and then deprotonated. The stretching vibrational band for ν(C=N) was detected between 1616 and 1596 cm^{-1} in complexes. A lower shift in the stretching frequency of ν(C=N) was observed in comparison to the free ligand, which was detected at 1629–1625 cm^{-1}, because of the interaction of the nitrogen atom with the metal center through the azomethine [52]. As a result of complex formation, the ν(N-N) band relocates from 1091–1076 cm^{-1} to 1046–1024 cm^{-1}, showing a decrease in the repulsive forces between the lone pairs of electrons on the nitrogen [53]. The identification of the distinctive vibrational frequencies at 594–530 cm^{-1} and 474–442 cm^{-1} corresponding to ν(Sn-N) and ν(Sn-O), offered additional proof for the successful formation of diorganotin(IV) complexes [54]. The outcomes attained are provided in Figures S34–S40. The IR spectra reveal that the ligands interact with tin metal in a tridentate manner.

3.6 | Mass Spectrometry

The mass spectra reveal the molecular weights of the compounds. In the mass spectra of the ligands (**1–3**), $[M + H]^+$ molecular ion peak emerged at *m/z* 353.0410, 363.1169, and 441.0923, respectively, which is in good agreement with its anticipated molecular weight. Complexes (**4–15**) exhibited a prominent molecular ion peak along with a characteristic tin (Sn) peak pattern.

TABLE 1 | Structure refinement and crystal data for compound **9**.

Structural parameter	Compound 9
CCDC no.	2376430
Empirical formula	$C_{20}H_{24}ClN_2O_4Sn$
Formula weight	510.55
Temperature/K	150.00(10)
Crystal system	Triclinic
Space group	P-1
a/Å	9.9660(10)
b/Å	10.2224(7)
c/Å	11.5464(9)
α/°	88.756(6)
β/°	69.703(8)
γ/°	67.701(8)
Volume/Å3	1012.54(16)
Z	2
ρ_{calc}g/cm^3	1.675
μ/mm^{-1}	11.499
F(000)	514.0
Crystal size/mm^3	0.548 × 0.164 × 0.118
Radiation	Cu Kα (λ = 1.54184)
2Θ range for data collection/°	8.23 to 138.696
Index ranges	$-12 \le h \le 8$, $-12 \le k \le 12$, $-13 \le l \le 12$
Reflections collected	5404
Independent reflections	3676 [R_{int} = 0.0330, R_{sigma} = 0.0425]
Data/restraints/parameters	3676/0/257
Goodness-of-fit on F_2	1.093
Final R indexes [$I \ge 2\sigma(I)$]	R_1 = 0.0414, wR_2 = 0.1066
Final R indexes [all data]	R_1 = 0.0430, wR_2 = 0.1095
Largest diff. peak/hole/e Å^{-3}	1.16/−1.83

The presence of the distinct tin isotope peak pattern across the different segments of complexes (**4–15**) indicates successful binding of Sn to the ligands. The mass spectra of synthesized compounds are provided in Figures S41–S53.

3.7 | X-Ray Crystallography

An appropriate single crystal of compound **9** was grown in hexane and chloroform to identify the geometry of the complex and validate the bonding of the hydrazone ligands to the tin metal. Based on the X-ray crystallography investigation, compound **9** formed in a triclinic cell with space group P-1 (no. 2), a = 9.9660(10) Å, b = 10.2224(7) Å, c = 11.5464(9) Å, α = 88.756(6)°, β = 69.703(8)°, γ = 67.701(8)°. Figure 1 shows the ORTEP plot of compound **9**. For compound **9**, the value of $\tau = (b - a)/60$ (where b is the greatest and a is the second highest basal angle around the Sn atom) is 0.11. This shows that the tin atom is surrounded by a distorted square pyramidal geometry [55]. The angles O3-Sn-N1 and O2-Sn-N1 are 81.92° and 70.96°, respectively, smaller than the ideal square pyramidal geometry. C10-Sn1-O2 bond angle is 91.64°, which is almost equal to the 90° of the ideal square pyramidal geometry [56]. The metal-nitrogen bond Sn(1)-N(1) has the longest bond length among the metal coordination bonds, measuring 2.220(3) Å; the metal-oxygen bond lengths, Sn-O3 and Sn-O2, are the shortest at 2.207(3) and 2.212(3) Å. Table 1 and 2 outline the most important geometrical parameters. The results of the X-ray crystallographic investigations on compound **9** were in full agreement with the previously indicated spectroscopic suggestions.

3.8 | Antimicrobial Activity

To identify potential pharmaceutical drugs with strong antimicrobial properties capable of fighting with a variety of microorganisms, synthesized compounds underwent *in vitro* testing to determine their efficacy against a spectrum of pathogens, four bacterial (*Bacillus subtilis* (MTCC 441), *Bacillus cereus* (MTCC 1305), *Pseudomonas aeruginosa* (MTCC 424), *Escherichia coli* (MTCC 732)) and two fungal (*Aspergillus niger* (MTCC 9933) and *Candida albicans* (MTCC 227)) strains. The screening employed the serial dilution approach with ciprofloxacin and fluconazole as standard medications. Table 3 displayed the result as minimum inhibitory concentration (MIC) in μmol/mL and the graphical representation is illustrated in Figure S54. The antimicrobial activity of the ligands was observed in the following order: **3** > **2** > **1**. Based on the observed data, it can be inferred that hydrazone ligand **3** with MIC values ranging from 0.0282 to 0.0141 μmol/mL had superior activity because of the stronger electron-withdrawing capabilities of the nitro and bromo groups relative to other functional groups. The azomethine linkage (>C=N-) in the compounds has been observed to inhibit microbial growth. Diorganotin(IV) complexes demonstrated greater activity in comparison to the hydrazone ligands. Tweedy chelation theory states that complexation increases the hydrophobic and lipophilic characteristics of the complexes, leading to an increase in their activity. Compounds having higher lipophilic characteristics have the benefit of easily passing *via* the lipid bilayer of cell membranes [57]. This makes it possible for them to efficiently obstruct active metal binding sites, which impedes the production of proteins and other biological activities within cells [58, 59]. The phenyl complexes exhibited superior activity having MIC values in the region from 0.0050 to 0.0043 μmol/mL as compared with other complexes against *E. coli* and *C. albicans*. This effect may result from the delocalization of π-electrons and the lipid-soluble property of tin atoms, which facilitates

TABLE 2 | Bond lengths (Å) and bond angles (°) for compound **9**.

Atom	Atom	Length/Å	Bond			Angle (deg.)
Sn1	O3	2.108(3)	O3	Sn1	N1	73.72(12)
Sn1	O3	2.207(3)	O3	Sn1	O2	152.94(10)
Sn1	O2	2.212(3)	O3	Sn1	N1	82.01(11)
Sn1	N1	2.220(3)	O2	Sn1	N1	70.92(11)
Sn1	C10	2.107(4)	C10	Sn1	O3	93.51(14)
Sn1	C11	2.110(4)	C10	Sn1	O2	91.67(14)
Cl1	C3	1.745(4)	C10	Sn1	N1	100.50(14)
O4	C17	1.384(4)	C10	Sn1	C11	159.61(17)
O4	C19	1.447(5)	C11	Sn1	O3	93.94(13)
O3	C18	1.334(5)	C11	Sn1	O2	90.29(14)
O2	C9	1.285(5)	C11	Sn1	N1	99.32(14)
O1	C6	1.367(5)				

TABLE 3 | Results of *in vitro* antimicrobial activity of compounds (**1**–**15**) expressed in terms of MIC (μmol/mL).

	Gram +ve bacteria		Gram −ve bacteria		Fungi	
MIC in μmol/mL Compound no.	***B. cereus***	***B. subtilis***	***E. coli***	***P. aeruginosa***	***A. niger***	***C. albicans***
1	0.0354	0.0177	0.0354	0.0354	0.0177	0.0177
2	0.0344	0.0344	0.0172	0.0344	0.0344	0.0172
3	0.0282	0.0141	0.0141	0.0282	0.0141	0.0141
4	0.0249	0.0249	0.0124	0.0249	0.0249	0.0124
5	0.0236	0.0118	0.0118	0.0236	0.0236	0.0118
6	0.0213	0.0106	0.0053	0.0106	0.0106	0.0053
7	0.0100	0.0100	**0.0050**	0.0100	0.0100	**0.0050**
8	0.0244	0.0122	0.0122	0.0244	0.0122	0.0122
9	0.0115	0.0231	0.0115	0.0115	0.0231	0.0115
10	0.0210	0.0100	0.0052	0.0100	0.0100	0.0052
11	0.0196	0.0098	**0.0049**	0.0098	0.0098	**0.0049**
12	0.0211	0.0211	0.0105	0.0105	0.0211	0.0105
13	0.0202	0.0101	0.0101	0.0101	0.0202	0.0101
14	0.0185	0.0092	0.0046	0.0092	0.0092	0.0046
15	0.0087	0.0087	**0.0043**	0.0087	0.0087	**0.0043**
Ciprofloxacin	0.0047	0.0047	0.0047	0.0047	—	—
Fluconazole	—	—	—	—	0.0051	0.0051

TABLE 4 | The IC_{50} values (μM) for synthetic compounds (**1**–**15**) against MCF7, A549, and HEK 293T cancer cell lines.

	IC_{50} values (μM ± SD)		
Compounds	**MCF7**	**A549**	**HEK 293T**
1	31.68 ± 2.78	33.56 ± 3.11	—
2	31.98 ± 3.43	34.87 ± 2.23	—
3	**26.07 ± 2.81**	**27.98 ± 2.76**	**90.66 ± 3.51**
4	46.27 ± 4.79	44.89 ± 5.04	—
5	**24.83 ± 2.52**	**28.66 ± 3.36**	**85.75 ± 3.01**
6	27.3 ± 3.85	29.96 ± 2.89	—
7	30.41 ± 2.18	35.48 ± 2.53	—
8	33.95 ± 5.27	29.97 ± 3.64	—
9	30.47 ± 4.32	34.08 ± 4.02	—
10	29.49 ± 3.04	31.34 ± 4.94	—
11	33.88 ± 5.09	30.89 ± 4.57	—
12	29.17 ± 1.94	34.48 ± 2.88	—
13	29.26 ± 2.03	33.62 ± 2.89	—
14	37.86 ± 4.66	42.38 ± 4.89	—
15	33.49 ± 3.41	30.78 ± 3.73	—
Doxorubicin	1.37 ± 0.28	1.02 ± 0.18	—

their penetration into microbial cells [60, 61]. Overall, the entire trend in the antimicrobial activity of complexes was diphenyl > dibutyl > diethyl > dimethyl. In summary, complexes **7**, **11**, and **15** having MIC values between 0.0043 and 0.0050 μmol/mL exhibit better effectiveness against *E. coli* and *C. albicans* strains equivalent to standard drugs ciprofloxacin (0.0047 μmol/mL) and fluconazole (0.0051 μmol/mL). The antimicrobial activity of compounds is increased when electron-withdrawing groups are incorporated into the aromatic ring as compared with electron-donating groups. The synthesized compounds revealed greater antimicrobial efficacy as compared with other comparable Sn compounds. These substances could be helpful in the development of medications known as antimicrobials, which treat microbial infections [62].

3.9 | Anticancer Activity

The anticancer potency of synthesized compounds (**1**–**15**) was assessed against three cancer cell lines: the A549 (human lung carcinoma cell line), MCF7 (human breast carcinoma cell line), and HEK 293T (normal human embryonic kidney cell line) using MTT-based assay. To comprehend the cytotoxicity of compounds in cancerous cells, IC_{50} values, that is, concentration of compounds where 50% cell death occurred, were calculated for all synthesized compounds and listed in Table 4. Graphical representation is provided in Figure S55. Out of all the compounds assessed against A549, MCF-7, and HEK 293T cell lines, the majority of the compounds exhibit noteworthy activity, the best activity was demonstrated by compound **3** (IC_{50} = 26.07 ± 2.81 μM, 27.98 ± 2.76 μM, and 90.66 ± 3.51 μM) and compound **5** (IC_{50} = 24.83 ± 2.52 μM, 28.66 ± 3.36 μM, and 85.75 ± 3.01 μM) against MCF7, A549, and HEK 293T, respectively. The most active compounds **3** and **5** underwent additional testing against normal cell line HEK 293T, and these compounds were shown to be nontoxic on normal cell line indicating their potential for use in further drug development. Compound **5** (IC_{50} value = 24.83 ± 2.52 μM, 28.66 ± 3.36 μM) demonstrated comparable efficacy to standard medicine doxorubicin (IC_{50} value = 1.37 ± 0.28 μM, 1.02 ± 0.18 μM) against MCF7 and A549 cell lines, respectively, indicating its potential as an anticancer agent. The comparison with other related Sn compounds showed that the synthesized compounds demonstrated superior anticancer activity [63].

4 | Conclusions

Twelve new diorganotin(IV) complexes using 2-(4-chloro-2-methylphenoxy)acetohydrazide hydrazones were synthesized and structurally studied using various spectroscopic techniques. An analysis of compound **9** using X-ray crystallography revealed that the tridentate hydrazone ligand was coupled to the tin atoms *via* the enolic-O, imine-N, and phenolic-O atoms, forming a distorted square pyramidal geometry. The synthesized compounds were explored for their *in vitro* antimicrobial activity, and findings disclosed that compounds **7**, **11**, and **15** with MIC values ranging from 0.0043 to 0.0050 μmol/mL were prospective antimicrobial agents. The outcomes of *in vitro* antimicrobial experiments corroborated the widely accepted hypothesis of chelation and overtone concept. Further, to determine the potential of the synthesized compounds as anticancer agents, we carried out *in vitro* anticancer investigations. Compound **3** (IC_{50} = 26.07 ± 2.81 μM, 27.98 ± 2.76 μM) and compound **5** (IC_{50} = 24.83 ± 2.52 μM, 28.66 ± 3.36 μM) exhibited the highest level of activity among the examined compounds, and their potential as anticancer agents was further assessed against normal cell line HEK 293T. The results of this work indicate that the hydrazone ligands and related diorganotin(IV) complexes have significant antimicrobial and anticancer potential. However, more research on the mechanisms of action and *in vivo* investigations are needed to fully comprehend the activity of the synthesized compounds.

Author Contributions

Pinki Barwa: writing – original draft, conceptualization, data curation, methodology, investigation. **Sonika Asija:** supervision, formal analysis, validation. **Yogesh Deswal:** writing – review and editing, software, data curation, validation, **Deepak Kumar:** anticancer evaluation. **Deepak Kumar Jindal:** anticancer evaluation. **Sandip Ghosh:** anticancer evaluation. **Biswarup Basu:** anticancer evaluation. **Shikha Poonia:** formal analysis. **Anju Ragshaniya:** formal analysis.

Acknowledgments

The author Pinki Barwa, SRF (09/752(0120)/2021-EMR-I) expresses her gratitude to Department of Chemistry and APJ Abdul Kalam Central instrumentation laboratory, Guru Jambheshwar University of Science & Technology, Hisar, India, for furnishing the necessary research facilities.

Conflicts of Interest

The authors declare no conflicts of interest.

Data Availability Statement

The data generated in this work are available upon request from the corresponding author.

References

1. G. Muteeb, M. T. Rehman, M. Shahwan, and M. Aatif, "Origin of Antibiotics and Antibiotic Resistance, and Their Impacts on Drug Development: A Narrative Review," *Pharmaceuticals* 16 (2023): 1615.

2. I. Ali, W. A. Wani, K. Saleem, and A. Haque, "Platinum Compounds: A Hope for Future Cancer Chemotherapy," *Anti-Cancer Agents in Medicinal Chemistry* 13 (2013): 296–306.

3. T. C. Johnstone, K. Suntharalingam, and S. J. Lippard, "The Next Generation of Platinum Drugs: Targeted Pt(II) Agents, Nanoparticle Delivery, and Pt(IV) Prodrugs," *Chemical Reviews* 116 (2016): 3436–3486.

4. M. Callari, J. R. Aldrich-Wright, P. L. de Souza, and M. H. Stenzel, "Polymers With Platinum Drugs and Other Macromolecular Metal Complexes for Cancer Treatment," *Progress in Polymer Science* 39 (2014): 1614–1643.

5. R. Sharma, V. J. Singh, and P. A. Chawla, "Advancements in the Use of Platinum Complexes as Anticancer Agents," *Anti-Cancer Agents in Medicinal Chemistry* 22 (2022): 821–835.

6. Y. Deswal, S. Asija, A. Dubey, et al., "Cobalt(II), Nickel(II), Copper(II) and Zinc(II) Complexes of Thiadiazole Based Schiff Base Ligands: Synthesis, Structural Characterization, DFT, Antidiabetic and Molecular Docking Studies," *Journal of Molecular Structure* 1253 (2022): 132266.

7. R. Oun, Y. E. Moussa, and N. J. Wheate, "The Side Effects of Platinum-Based Chemotherapy Drugs: A Review for Chemists," *Dalton Transactions* 47 (2018): 6645–6653.

8. C. A. Rabik and M. E. Dolan, "Molecular Mechanisms of Resistance and Toxicity Associated With Platinating Agents," *Cancer Treatment Reviews* 33 (2007): 9–23.

9. Y. Deswal, S. Asija, D. Kumar, et al., "Transition Metal Complexes of Triazole-Based Bioactive Ligands: Synthesis, Spectral Characterization, Antimicrobial, Anticancer and Molecular Docking Studies," *Research on Chemical Intermediates* 48 (2022): 703–729.

10. P. B. Tchounwou, S. Dasari, F. K. Noubissi, P. Ray, and S. Kumar, "Advances in Our Understanding of the Molecular Mechanisms of Action of Cisplatin in Cancer Therapy," *Journal of Experimental Pharmacology* 13 (2021): 303–328.

11. A. Alama, B. Tasso, F. Novelli, and F. Sparatore, "Organometallic Compounds in Oncology: Implications of Novel Organotins as Antitumor Agents," *Drug Discovery Today* 14 (2009): 500–508.

12. I. Ott and R. Gust, "Non Platinum Metal Complexes as Anti-Cancer Drugs," *Archiv der Pharmazie: An International Journal Pharmaceutical and Medicinal Chemistry* 340 (2007): 117–126.

13. Y. Deswal, S. Asija, A. Tufail, et al., "Metal Complexes of 1,2,4-Triazole Based Ligand: Synthesis, Structural Elucidation, DFT Calculations, Alpha-Amylase and Alpha-Glucosidase Inhibitory Activity Along With Molecular Docking Studies," *Journal of Inorganic and Organometallic Polymers and Materials* 34 (2024): 144–160.

14. F. Arjmand, S. Parveen, S. Tabassum, and C. Pettinari, "Organo-Tin Antitumor Compounds: Their Present Status in Drug Development and Future Perspectives," *Inorganica Chimica Acta* 423 (2014): 26–37.

15. P. V. Simpson, N. M. Desai, I. Casari, M. Massi, and M. Falasca, "Metal-Based Antitumor Compounds: Beyond Cisplatin," *Future Medicinal Chemistry* 11 (2019): 119–135.

16. S. Ramos-Inza, D. Plano, and C. Sanmartin, "Metal-Based Compounds Containing Selenium: An Appealing Approach Towards Novel Therapeutic Drugs With Anticancer and Antimicrobial Effects," *European Journal of Medicinal Chemistry* 244 (2022): 114834.

17. A. M. Florea, E. Dopp, and D. Busselberg, "Elevated Ca^{2+} Transients Induced by Trimethyltin Chloride in HeLa Cells: Types and Levels of Response," *Cell Calcium* 37 (2005): 251–258.

18. S. Fani, F. Dehghan, H. Karimian, et al., "Monobenzyltin Complex C1 Induces Apoptosis in MCF-7 Breast Cancer Cells Through the Intrinsic Signaling Pathway and Through the Targeting of MCF-7-Derived Breast Cancer Stem Cells via the Wnt/β-Catenin Signaling Pathway," *PLoS ONE* 11 (2016): e0160836.

19. M. Sirajuddin and S. Ali, "Organotin(IV) Carboxylates as Promising Potential Drug Candidates in the Field of Cancer Chemotherapy," *Current Pharmaceutical Design* 22 (2016): 6665–6681.

20. H. Ullah, V. Previtali, H. B. Mihigo, et al., "Structure-Activity Relationships of New Organotin(IV) Anticancer Agents and Their Cytotoxicity Profile on HL-60, MCF-7 and HeLa Human Cancer Cell Lines," *European Journal of Medicinal Chemistry* 181 (2019): 111544.

21. Q. Li, M. F. C. Guedes da Silva, and A. J. Pombeiro, "Diorganotin(IV) Derivatives of Substituted Benzohydroxamic Acids With High Antitumor Activity," *Chemistry—A European Journal* 10 (2004): 1456–1462.

22. M. S. Ahmad, M. Hussain, M. Hanif, S. Ali, and B. Mirza, "Synthesis, Chemical Characterization and Biological Screening for Cytotoxicity and Antitumor Activity of Organotin(IV) Derivatives of 3,4-Methylenedioxy 6-Nitrophenylpropenoic Acid," *Molecules* 12 (2007): 2348–2363.

23. H. Yin, H. Liu, and M. Hong, "Synthesis, Structural Characterization and DNA-Binding Properties of Organotin(IV) Complexes Based on Schiff Base Ligands Derived From 2-Hydroxy-1-Naphthaldy and 3- or 4-Aminobenzoic Acid," *Journal of Organometallic Chemistry* 713 (2012): 11–19.

24. J. H. Huang and E. Matzner, "Degradation of Organotin Compounds in Organic and Mineral Forest Soils," *Journal of Plant Nutrition and Soil Science* 167 (2004): 33–38.

25. M. Gajewska, K. V. Luzyanin, M. F. C. Guedes da Silva, Q. Li, J. Cui, and A. J. Pombeiro, "Cyclic Trinuclear Diorganotin(IV) Complexes—The First Tin Compounds Bearing Oximehydroxamate Ligands: Synthesis, Structural Characterization and High In Vitro Cytotoxicity," *European Journal of Inorganic Chemistry* 25 (2009): 3765–3769.

26. M. Martins, P. V. Baptista, A. S. Mendo, et al., "In Vitro and In Vivo Biological Characterization of the Anti-Proliferative Potential of a Cyclic Trinuclear Organotin (Iv) Complex," *Molecular BioSystems* 12 (2016): 1015–1023.

27. G. N. KaluCerovic, R. Paschke, S. Prashar, and S. Gomez-Ruiz, "Synthesis, Characterization and Biological Studies of 1-D Polymeric Triphenyltin(IV) Carboxylates," *Journal of Organometallic Chemistry* 695 (2010): 1883–1890.

28. Y. Ellahioui, S. Prashar, and S. Gomez-Ruiz, "Anticancer Applications and Recent Investigations of Metallodrugs Based on Gallium, Tin and Titanium," *Inorganics* 5 (2017): 4.

29. P. G. Avaji, C. V. Kumar, S. A. Patil, K. Shivananda, and C. Nagaraju, "Synthesis, Spectral Characterization, In-Vitro Microbiological Evaluation and Cytotoxic Activities of Novel Macrocyclic Bis Hydrazone," *European Journal of Medicinal Chemistry* 44 (2009): 3552–3559.

30. P. Vicini, F. Zani, P. Cozzini, and I. Doytchinova, "Hydrazones of 1,2-Benzisothiazole Hydrazides: Synthesis, Antimicrobial Activity and QSAR Investigations," *European Journal of Medicinal Chemistry* 37 (2002): 553–564.

31. M. S. S. Khan, M. A. Salam, R. S. Haque, et al., "Synthesis, Cytotoxicity, and Long-Term Single Dose Anti-Cancer Pharmacological Evaluation of Dimethyltin(IV) Complex of *N*(4)-Methylthiosemicarbazone (Having ONS Donor Ligand)," *Cogent Biology* 2 (2016): 1154282.

32. N. Kumar, S. Asija, Y. Deswal, et al., "Exploring Diorganotin (IV) Complexes of Hydrazone Based Ligands as Multi-Target Agents: Synthesis, Structural Characterization, DFT and In Vitro Biological Evaluation," *Inorganic Chemistry Communications* 161 (2024): 112120.

33. O. V. Dolomanov, L. J. Bourhis, R. J. Gildea, J. A. K. Howard, and H. Puschmann, "F25A, F26A, F27A, F30A, F28A, F29A, F25, F26, F27, F28, F29, F30 With Sigma for 1-2 Distances of 0.01 and Sigma for 1-3 Distances of 0.01 P5A, P5 With Sigma for 1-2 Distances of 0.01 and Sigma for 1-3 Distances of 0.01 F10A, F7A, F10, F12, F9, F11A, F7, F12A, F8, F9A, F11, F8A," *Journal of Applied Crystallography* 42 (2009): 339–341.

34. G. M. Sheldrick, "SHELXT-Integrated Space-Group and Crystal-Structure Determination," *Acta Crystallographica Section A: Foundations and Advances* A71 (2015): 3–8.

35. P. Barwa, S. Asija, Y. Deswal, and J. S. Kirar, "Investigating the Antimicrobial Potential of Diorganotin(IV) Complexes Incorporating Hydrazone Ligands: Synthesis, Structural Elucidation, X-Ray Crystallography, DFT, and Antimicrobial Activity," *Inorganica Chimica Acta* 564 (2024): 121941.

36. P. Barwa, S. Asija, Y. Deswal, N. Kumar, A. Kumar, and J. Devi, "New Pentacoordinated Diorganotin(IV) Complexes of o-Aminophenol Based Schiff Base Ligands: Synthesis, Characterization, Antioxidant, Antimicrobial and Molecular Docking Studies," *Research on Chemical Intermediates* 49 (2023): 3411–3440.

37. I. Sindhu and A. Singh, "Experimental and Theoretical Insight of Schiff Base Transition Metal Complexes: Synthesis, Characterization, Antimicrobial and COVID-19 Molecular Docking Studies," *Research on Chemical Intermediates* 50 (2024): 413–436.

38. T. Mosmann, "Rapid Colorimetric Assay for Cellular Growth and Survival: Application to Proliferation and Cytotoxicity Assays," *Journal of Immunological Methods* 65 (1983): 55–63.

39. D. Kumar, G. Mariappan, A. Husain, J. Monga, and S. Kumar, "Design, Synthesis and Cytotoxic Evaluation of Novel Imidazolone Fused Quinazolinone Derivatives," *Arabian Journal of Chemistry* 10 (2017): 344–350.

40. S. Saroya, S. Asija, Y. Deswal, et al., "Pentacoordinated Diorganotin(IV) Complexes of Schiff Base Ligands: Synthesis, Characterization, Antimicrobial and Anticancer Studies," *Research on Chemical Intermediates* 48 (2022): 4671–4691.

41. S. A. Patra, G. Sahu, D. Mohapatra, P. D. Pattanayak, and R. Dinda, "Fluorescent Diorganotin(IV) Complexes as Anticancer Agents: Study of Cytotoxicity, Cellular Localization, and Mechanism of Cell Death," *Organometallics* 42 (2023): 1934–1950.

42. N. Kumar, S. Asija, Y. Deswal, et al., "Insighting the Inhibitory Potential of New Diorganotin(IV) Complexes Derived From Tridentate Ligands: Synthesis, Structural Elucidation and Biological Evaluation," *Inorganic Chemistry Communications* 154 (2023): 110953.

43. P. Khatkar and S. Asija, "New Diorganotin(IV) Complexes of Tridentate Schiff Bases Derived From 1,3-Indanedione Derivative: Synthesis, Spectral Studies and In Vitro Antimicrobial Activities," *Phosphorus, Sulfur, and Silicon and the Related Elements* 192 (2017): 446–453.

44. S. Saroya, S. Asija, Y. Deswal, N. Kumar, and A. Kumar, "Synthesis, Spectral Studies, In Vitro Antimicrobial Activity and Molecular Docking Studies of Organotin(IV) Complexes Derived From Tridentate Schiff Base Ligands," *Research on Chemical Intermediates* 48 (2022): 2949–2971.

45. S. Kumar and M. Nath, "New Diorganotin(IV) Complexes of Salicylaldehyde Based Hydrazones Bearing Furan Heterocycle Moiety: X-Ray Structural Investigation of Dimethyltin (IV) and Diphenyltin (IV) Complexes," *Journal of Organometallic Chemistry* 856 (2018): 87–99.

46. T. P. Lockhart and W. F. Manders, "Structure Determination by NMR Spectroscopy. Dependence of |2J (119Sn, 1H)| on the Me-Sn-Me Angle in Methyltin(IV) Compounds," *Inorganic Chemistry* 25 (1986): 892–895.

47. S. Saroya, S. Asija, N. Kumar, and Y. Deswal, "Organotin (IV) Complexes Derived From Tridentate Schiff Base Ligands: Synthesis, Spectroscopic Analysis, Antimicrobial and Antioxidant Activity," *Journal of the Indian Chemical Society* 99 (2022): 100379.

48. N. Kumar, S. Asija, Y. Deswal, S. Saroya, A. Kumar, and J. Devi, "Organotin(IV) Complexes Derived From Hydrazone Ligands: Synthesis, Spectral Analysis, Antimicrobial and Molecular Docking Studies," *Phosphorus, Sulfur, and Silicon and the Related Elements* 197 (2021): 952–963.

49. H. J. Kroth, H. Schumann, H. G. Kuivila, C. D. Schaeffer, Jr., and J. J. Zuckerman, "Tin-119 Chemical Shifts of Ortho, Meta, Para, 2,6-, and Polysubstituted Aryltrimethyltin Derivatives and Related Organotin Compounds," *Journal of the American Chemical Society* 97 (1975): 1754–1760.

50. S. Shujah, S. Ali, N. Khalid, M. J. Alam, S. Ahmad, and A. Meetsma, "Synthesis, Spectroscopic Characterization, X-Ray Structure, DFT Calculations, and Antimicrobial Studies of Diorganotin(IV) Complexes of Monotopic Oxygen Nitrogen Donor Schiff Base," *Chemical Papers* 72 (2018): 903–919.

51. S. Ahsen, I. Tanvir, N. Uddin, et al., "Synthesis, Structural Elucidation and Anticancer Activity of Diorganotin(IV) Complexes Derived From Isonicotinoyl Hydrazones," *Inorganica Chimica Acta* 564 (2024): 121965.

52. A. A. Kubaisi and K. Z. Ismail, "Nickel(II) and Palladium(II) Chelates of Dehydroacetic Acid Schiff Bases Derived From Thiosemicarbazide and Hydrazinecarbodithioate," *Canadian Journal of Chemistry* 72 (1994): 1785–1788.

53. S. Ramzan, S. Shujah, K. B. Holt, et al., "Structural Characterization, DNA Binding Study, Antioxidant Potential and Antitumor Activity of Diorganotin(IV) Complexes Against Human Breast Cancer Cell Line MDA-MB-231," *Journal of Organometallic Chemistry* 990 (2023): 122671.

54. S. Poonia, S. Asija, Y. Deswal, and J. S. Kirar, "Exploring the Microbial Inhibition Ability of Newly Synthesized Diorganotin(IV) Complexes of Hydrazone Ligands: Structural Elucidation, Crystal Structure, and DFT Studies," *Applied Organometallic Chemistry* 38 (2024): e7704.

55. P. Debnath, K. S. Singh, T. S. Devi, et al., "Synthesis, Characterization, Crystal Structures and Anti-Diabetic Activity of Organotin(IV) Complexes With 2-(4-Hydroxynaphthylazo)-Benzoic Acid," *Inorganica Chimica Acta* 510 (2020): 119736.

56. M. A. El-Bindary and A. A. El-Bindary, "Synthesis, Characterization, DNA Binding, and Biological Action of Dimedone Arylhydrazone Chelates," *Applied Organometallic Chemistry* 36 (2022): e6576.

57. Z. H. Chohan, A. Scozzafava, and C. T. Supuran, "Zinc Complexes of Benzothiazole-Derived Schiff Bases With Antibacterial Activity," *Journal of Enzyme Inhibition and Medicinal Chemistry* 18 (2003): 259–263.

58. P. Khatkar, A. Ahlawat, S. Asija, and V. Singh, "Synthesis, Characterization, In Vitro Antimicrobial, DNA Binding Activity and QSAR Studies of Diorganotin(IV) Complexes of Schiff Bases Derived From 2-Benzoyl-1 H-Indene-1,3(2 H)-Dione and 4-Substituted Benzoic Acid Hydrazides," *Phosphorus, Sulfur, and Silicon and the Related Elements* 196 (2020): 133–145.

59. N. Kumar, S. Asija, Y. Deswal, S. Saroya, and A. Kumar, "Development of New Tridentate Ligands Bearing Hydrazone Motif and Their Diorganotin(IV) Complexes: Synthesis, Spectral, Antimicrobial and Molecular Docking Studies," *Research on Chemical Intermediates* 48 (2022): 5133–5154.

60. S. Saroya, S. Asija, Y. Deswal, N. Kumar, and J. Devi, "Synthesis, Characterization, and In Vitro Antimicrobial and Antioxidant Study of the Pentacoordinated Organotin(IV) Complexes Based on Acid Hydrazide Schiff Base Ligands," *Pharmaceutical Chemistry Journal* 57 (2023): 1372–1383.

61. P. Khatkar, S. Asija, A. Ahlawat, and V. Singh, "Synthesis, Characterization, In Vitro Antimicrobial and QSAR Studies of Diorganotin(IV)

Complexes of Schiff Bases Derived From 2-(3-Methylbutanoyl)-1H-Indene-1,3(2H)-dione and 4-Substituted Anilines," *Monatshefte für Chemie-Chemical Monthly* 150 (2019): 207–218.

62. T. S. Basu Baul, "Antimicrobial Activity of Organotin(IV) Compounds: A Review," *Applied Organometallic Chemistry* 22 (2008): 195–204.

63. M. Sirajuddin, S. Ali, and M. N. Tahir, "Pharmacological Investigation of Mono-, Di- and Tri-Organotin(IV) Derivatives of Carbodithioates: Design, Spectroscopic Characterization, Interaction With SS-DNA and POM Analyses," *Inorganica Chimica Acta* 439 (2016): 145–158.

Supporting Information

Additional supporting information can be found online in the Supporting Information section.